Description of ionization in the molecular approach to atomic collisions

C. Harel, H. Jouin, and B. Pons
Laboratoire des Collisions Atomiques, Centre de Physique Théorique et Modélisation, URA 1537 du CNRS, Université de Bordeaux I, 351 Cours de Libération, 33405 Talence Cedex, France

L. F. Errea, L. Méndez, and A. Riera
Departamento de Química, C-IX, Universidad Autónoma de Madrid, Cantoblanco, E-28049 Madrid, Spain
(Received 1 April 1996)

Molecular treatments of atomic collisions have traditionally been restricted to low nuclear velocities because of their failure to reproduce the fall of the capture cross sections at higher velocities. The limitation has recently been seen to be due to their description of ionizing processes. This feature is shown here to be a general one for multicharged ion-atom collisions. Its origin and characteristics are described and illustrated for the prototypical $Li^{3+}+H(1s)$ reaction. Ionization appears as a result of the inertia of the electron cloud to adiabatically follow the nuclear motion. This gives rise to nonadiabatic transitions, which represent an ionizing flux whenever the nuclear velocity is high enough that the energy of the traveling molecular orbitals involved is positive in both moving atomic reference frames. Two strongly connected mechanisms appear, corresponding to the relative translational and rotational nuclear motions. Because of the finiteness of the basis, these mechanisms terminate with unphysical trapping effects. While interesting *per se*, knowledge of these features is also useful with respect to improving molecular treatments of atomic collisions with the addition of pseudostates. [S1050-2947(96)05312-7]

PACS number(s): 34.10.+x, 34.50.Fa, 34.70.+e

I. INTRODUCTION

The application of the molecular approach to atomic collisions was restricted for a long time to the low-impact velocity range because of its inability to reproduce the fall of charge-exchange cross sections at higher energies. In Refs. [1,2], using $He^{2+}+H$ collisions as a benchmark, the physical origin of this failure was ascribed to the description, by bound molecular states, of ionization processes, followed by a trapping of the corresponding flux, which persists in the asymptotic region, and produces an overestimation of capture probabilities. Although in some cases [3], the trapping effect affects excitation, for collisions between bare multicharged ions and $H(1s)$, it almost exclusively occurs for capture channels.

The previous information was employed in [4] to simultaneously calculate capture, excitation, and ionization cross sections in $He^{+}+H^{+}$ collisions. This reaction was chosen because it is characterized by a sudden mechanism at very short internuclear distances and the selection of pseudostates to complete the basis at these distances is simplest. In the other extreme we have reactions involving negative ions where ionization takes place for a wide range of distances. As a benchmark for these reactions, we studied [5] the case of $H^{+}+H^{-}$ collisions. It was seen that, although a judicious selection of exit probabilities allowed us to calculate capture and ionization cross sections, from the point of view of a systematic treatment the procedure is unsatisfactory: trapping could not be eliminated with any set of pseudostates available; indeed, most of the ionizing population was described by excited bound molecular states. In further (unpublished) work, we found that to a lesser extent the same holds for $He^{2+}+H(1s)$ collisions, which are good representatives of reactions involving multicharged ions.

From this previous work, we conclude that a reliable general procedure to construct pseudostates is not available at present. In particular, it is not sufficient to complete the close-coupling basis with a set of wave functions with a positive energy in the asymptotic region. Therefore, to offset the trapping effect requires a detailed investigation on the description of ionization by the molecular expansions, which is lacking in the literature. This is attempted in the present paper.

More specifically, the following points need clarification: (i) the basic reason why ionization is described by molecular expansions, modified or not by a common translation factor [6], but not by expansions modified with plane-wave factors; (ii) whether in actual calculations the corresponding flux describes genuine ionization, since otherwise the whole scheme proposed in [1,2] would be conjecture; (iii) the origin of the unphysical trapping effect; (iv) how general these features are in the treatment of atomic collisions; and (v) whether one may conclude on desirable general properties of pseudostates. A full answer to this last question would permit one to complete the molecular basis, so as to achieve convergence of the close-coupling molecular expansion in a way similar to that carried out, e.g., in [7] for atomic expansions.

To deal with points (i)–(v), the present work departs from our previous ones in that the character of the electronic cloud is explicitly examined rather than being worked on from analogy to alternative approaches. With respect to these approaches, it was noticed in [2] that a feature of particular importance is the promotion of the ionizing flux through transitions to increasingly diffuse multiplets; this was seen to be similar to the so-called T superseries transitions in the framework of the ''hidden crossing'' method [8–12]. A further connection was suggested in [2] with the classical findings of Bandarage and Parson [13], according to which at

very large internuclear separations many ionizing electrons are bound when viewed from a molecular frame. Now, although some analogies will be mentioned, explicit links with Refs. [8–13] would require a separate investigation, which will not be attempted here.

The next section introduces the main formal tools that are required in the analysis, which is contained in Sec. III. Prior to this analysis, we first show that our previous conclusions [2] for the $He^{2+}+H(1s)$ reaction also hold for $I^{Z+}+H(1s)$ (where I denotes ions with $Z=3$–6). Then, to choose a benchmark different from [2], we shall specifically refer to the $Li^{3+}+H(1s)$ reaction as a representative of multicharged ion+H($1s$) collisions. Atomic units will be employed unless otherwise specified.

II. IONIZING CHARACTER OF MOLECULAR STATES

A. Description of ionization in atomic collisions

We consider a one-electron problem in the impact-parameter approach. We call $\mathbf{R}$ the position vector of the projectile nucleus B (of charge Z_B) relative to the target nucleus A (of charge Z_A) and $\mathbf{r}_A,\mathbf{r}_B$ the electron position vector relative to A and B, respectively. The impact parameter equation is

$$(H-i\partial_0)\Psi=0, \tag{1}$$

where H is the Born-Oppenheimer electronic Hamiltonian and ∂_0 is the time derivative, taken by keeping fixed the electron position vector $\mathbf{r}$ with respect to an origin $\mathcal{O}$ that is situated at a distance pR of nucleus A and qR of nucleus B; in particular, for $p=0$, $\partial_0=\partial_A$ and for $p=1$, $\partial_0=\partial_B$. Each solution Ψ (see below) is a wave function representing the electronic state of the colliding system and the nuclei follow rectilinear trajectories $\mathbf{R}=\mathbf{b}+\mathbf{v}t$ with constant velocity $\mathbf{v}$ and impact parameter $\mathbf{b}$. The transition amplitude t_{if} to a given final state Φ_f when the initial state is represented by Φ_i is given by

$$t_{if}=\langle\Psi_f^-|\Psi_i^+\rangle=\lim_{t\to+\infty}\langle\Phi_f|\Psi_i^+\rangle, \tag{2}$$

where Ψ_i^+ is the solution of (1) that satisfies the outgoing boundary condition [14,15]

$$\begin{aligned}\Psi_i^+(\mathbf{r},t)&\underset{t\to-\infty}{\sim}\Phi_i^A(\mathbf{r},t)\\&=\phi_i^A(\mathbf{r})D_A\exp[-iE_i^At-iZ_A\\&\quad\times(1-Z_B)v^{-1}\ln(R-vt)],\end{aligned} \tag{3}$$

and for excitation (A) or charge exchange (B) processes, Ψ_f^- fulfills (1) with the ingoing condition

$$\begin{aligned}\Psi_f^-(\mathbf{r},t)&\underset{t\to+\infty}{\sim}\Phi_f^{A,B}(\mathbf{r},t)\\&=\phi_f^{A,B}(\mathbf{r})D_{A,B}\exp[-iE_i^{A,B}t-iZ_{A,B}\\&\quad\times(1-Z_{B,A})v^{-1}\ln(R-vt)].\end{aligned} \tag{4}$$

In (3) and (4) $\phi_n^{A,B}(\mathbf{r})$ ($n=i,f$) are (normalized) eigenfunctions of the arrangement channel Hamiltonian corresponding to atoms $(A+e^-),(B+e^-)$, respectively,

$$h_{A,B}\phi_n^{A,B}=E_n^{A,B}\phi_n^{A,B}, \tag{5}$$

with $E_n^{A,B}<0$, and

$$H\underset{\substack{R\to\infty\\r_B\to\infty}}{\sim}h_A,\quad H\underset{\substack{R\to\infty\\r_A\to\infty}}{\sim}h_B. \tag{6}$$

The plane-wave factors $D_{A,B}$ are given by

$$D_A=\exp\left(-ip\mathbf{v}\cdot\mathbf{r}-\frac{i}{2}p^2v^2t\right)=\exp\left(-ip\mathbf{v}\cdot\mathbf{r}_A+\frac{i}{2}p^2v^2t\right), \tag{7}$$

$$D_B=\exp\left(iq\mathbf{v}\cdot\mathbf{r}-\frac{i}{2}q^2v^2t\right)=\exp\left(iq\mathbf{v}\cdot\mathbf{r}_B+\frac{i}{2}q^2v^2t\right). \tag{8}$$

We note that the ingoing wave function also fulfills

$$(H_A'-\tfrac{1}{2}p^2v^2-i\partial_A)\Psi_f^-(\mathbf{r},t)=0. \tag{9}$$

with $H_A'=D_AHD_A^{-1}$ the fixed-nuclei Hamiltonian defined in the inertial frame moving with the velocity of nucleus A. Similarly, we have

$$(H_B'-\tfrac{1}{2}q^2v^2-i\partial_B)\Psi_f^-(\mathbf{r},t)=0, \tag{10}$$

with $H_B'=D_BHD_B^{-1}$. From (4) we see that Eq. (9) or (10) is trivially fulfilled for excitation (A) or exchange (B) arrangement channels, respectively, in the limit $t\to+\infty$, where $H_{A,B}'\to h_{A,B}'=D_{A,B}h_{A,B}D_{A,B}^{-1}$, since

$$\partial_A\Phi_f^A=-i\left[E_f^A-\tfrac{1}{2}p^2v^2-\frac{Z_A(1-Z_B)}{R}\right]\Phi_f^A, \tag{11}$$

$$\partial_B\Phi_f^B=-i\left[E_f^B-\tfrac{1}{2}q^2v^2-\frac{Z_B(1-Z_A)}{R}\right]\Phi_f^B, \tag{12}$$

and from (5) the final unperturbed states fulfill

$$h_{A,B}'\Phi_f^{A,B}=E_f^{A,B}\Phi_f^{A,B}, \tag{13}$$

where the atomic energies

$$E_f^{A,B}=\langle\Phi_f^{A,B}|h_{A,B}'|\Phi_f^{A,B}\rangle<0. \tag{14}$$

Above the ionization threshold, there is an additional arrangement channel corresponding to three (nuclei plus electron) unbound particles. For the pertinent non-L^2-integrable boundary condition corresponding to it, see, e.g., [16]. Here we are interested in Hilbert-space solutions of the problem, so that for large t the ionizing functions $\Phi_f(\mathbf{r},t)$ can be chosen to be any suitable orthonormal set of wave packets $\Phi_\alpha^{\rm ion}(\mathbf{r},t)$, formed by superpositions of generalized eigenvectors of (in principle, either) h_A' or h_B' in (13), such that they represent states that are unbound with respect to *both* atoms. It is unnecessary, in the present context, to further specify these eigendifferentials [14] describing the ionization process. They fulfill

$$E_\alpha^{\rm ion}=\langle\Phi_\alpha^{\rm ion}|h'_{A,B}|\Phi_\alpha^{\rm ion}\rangle>0 \tag{15}$$

for *both* Hamiltonians $h'_{A,B}$, in contrast to the proper (bound) eigensolutions of Eq. (13), for which either $E_f^A<0$ or $E_f^B<0$ [Eq. (14)].

Choosing, for example, the outgoing solution $\Psi_i^+(\mathbf{r},t)$, Eq. (1) should be integrated, starting from the initial condition (3), until a sufficiently large time such that the asymptotic orthogonality [15] between all exit states $\Phi_f(\mathbf{r},t)$ is fulfilled to good accuracy (i.e., such that the effect of overcompleteness of the atomic eigenfunctions is negligible). Then $\Psi_i^+(\mathbf{r},t)$ is of the form

$$\Psi_i^+(\mathbf{r},t)=\sum_n c_n^A(t)\Phi_n^A(\mathbf{r},t)+\sum_n c_n^B(t)\Phi_n^B(\mathbf{r},t)$$
$$+\sum_\alpha c_\alpha^{\rm ion}(t)\Phi_\alpha^{\rm ion}(\mathbf{r},t). \tag{16}$$

In practice, such a form applies to all times where overlap effects between the ''important'' reaction channels are small. A similar expression holds for the time-reversed solution Ψ_f^- for sufficiently large negative times. From asymptotic orthogonality and Eqs. (2) and (16) we then obtain the transition probabilities for excitation $P_n^A=|c_n^A(\infty)|^2$, charge transfer $P_n^B=|c_n^B(\infty)|^2$, and ionization $P^{\rm ion}=\Sigma_\alpha|c_\alpha^{\rm ion}(\infty)|^2$.

B. Molecular expansions

In a molecular close-coupling treatment, we solve Eq. (1) by expanding Ψ_i^+ in terms of a set of basis functions $\{e^{iU}\chi_n, n=1,\ldots,N\}$,

$$\Psi_i^+(\mathbf{r},t)\approx\exp[iU(\mathbf{r},t)]\sum_{n=1}^N a_n(t)\chi_n(\mathbf{r},R)$$
$$\times\exp\left[-i\int E_n(R)dt\right], \tag{17}$$

where χ_n represents an eigenstate of the fixed-nuclei Hamiltonian H, of energy E_n, or a pseudostate. The common translation factor [6] (CTF) $\exp(iU)$ in (17) fulfills the usual conditions

$$\exp[iU(\mathbf{r},t)]\underset{\substack{t\to\pm\infty\\ r_B/r_A\to\infty}}{\sim}D_A, \tag{18}$$

$$\exp[iU(\mathbf{r},t)]\underset{\substack{t\to\pm\infty\\ r_A/r_B\to\infty}}{\sim}D_B \tag{19}$$

and, upon a change of origin $\mathcal{O}\to\mathcal{O}'$, it changes to

$$\exp[iU'(\mathbf{r}',t)]=\exp[iU(\mathbf{r},t)]\exp\left[i(p-p')\mathbf{v}\cdot\mathbf{r}\right.$$
$$\left.+\frac{i}{2}(p-p')^2v^2t\right]. \tag{20}$$

In particular, from (7) we see that when the origin is shifted to nucleus A ($p'=0$), it becomes

$$\exp[iU_A(\mathbf{r}_A,t)]=\exp[iU(\mathbf{r},t)]D_A^{-1}, \tag{21}$$

and from (8), when it is shifted to nucleus B ($p'=1=p+q$),

$$\exp[iU_B(\mathbf{r}_B,t)]=\exp[iU(\mathbf{r},t)]D_B^{-1}. \tag{22}$$

It is well known [14,17] that substitution of the ansatz (17) in Eq. (1) leads to a set of coupled differential equations for the expansion coefficients a_n that is equivalent to a variational treatment for

$$\delta I=\delta\int\langle\Psi_i^+|H-i\partial_0|\Psi_i^+\rangle dt=0, \tag{23}$$

within the manifold spanned by the set $\{\chi_n(\mathbf{r},R); n=1,\ldots,N\}$, and the resulting transition probabilities are accurate to order $\|\delta\Psi_i^+\|^2$, where $\delta\Psi_i^+$ is the error function. As the method minimizes this error function, it will try to reproduce, in the domain of internuclear distances where overlap effects are small, the three kind of terms (excitation, charge exchange, and ionization) appearing in the form (16). Then, we see from Eq. (14) that a basis function $e^{iU}\chi_n$ such that

$$E_n^{(A)}=\langle e^{iU}\chi_n|h'_A|e^{iU}\chi_n\rangle=\langle e^{iU_A}\chi_n|h_A|e^{iU_A}\chi_n\rangle \tag{24}$$

is negative describes (elastic or) excitation channels; the second set of angular brackets in (24) arises from the definition of h'_A and Eq. (21). Similarly, when

$$E_n^{(B)}=\langle e^{iU}\chi_n|h'_B|e^{iU}\chi_n\rangle=\langle e^{iU_B}\chi_n|h_B|e^{iU_B}\chi_n\rangle \tag{25}$$

is negative, the basis function $e^{iU}\chi_n$ represents charge exchange. Finally, from (15), when *both* $E_n^{(A)}(R;b,v)$ and $E_n^{(B)}(R;b,v)$ are positive, it describes ionization. We notice that (24) and (25) are origin-independent quantities and when χ_n is a bound eigenfunction of H, the corresponding molecular energy $E_n(R)<0$.

We may now distinguish molecular treatments with and without pseudostates. In the present work we are interested in the latter, for which, for large enough t, all molecular functions are such that either $E_n^{(A)}<0$ or $E_n^{(B)}<0$. For instance, when $\chi_n\to\phi_n^A$ as $R\to\infty$, from (24), (18), (21), and (5) we have

$$E_n^{(A)}=\langle e^{iU_A}\chi_n|h_A|e^{iU_A}\chi_n\rangle\to\langle e^{iU_A}\phi_n^A|h_A|e^{iU_A}\phi_n^A\rangle$$
$$=\langle\phi_n^A|h_A|\phi_n^A\rangle=E_n^A<0 \tag{26}$$

in this limit, with the similar result $E_n^{(B)}\to E_n^B<0$ when $\chi_n\to\phi_n^B$ and $R\to\infty$. Consequently, even when ionization is described during the collision, because for some n we have $E_n^{(A,B)}(R;b,v)>0$, if the integration is carried out to a sufficiently large time and in the absence of pseudostates, the corresponding flux will eventually be trapped in either excitation $[E_n^{(A)}(R;b,v)<0]$ or charge-exchange $[E_n^{(B)}(R;b,v)<0]$ channels. Therefore, a proper separation between excitation, exchange, and ionization probabilities requires separating trapped from ''genuine'' transition probabilities, which may or may not be feasible in practice without ambiguities.

C. Other expansions

Similar reasonings apply to a CTF-modified atomic expansion [2]. The same holds for a molecular expansion with-

out translation factors, which, for any finite-time interval $[-t_M,+t_M]$, can formally be taken as a special case of expansion (17) in which a strong cutoff is introduced in the CTF. Of course, because of Galilean invariance (20), this can only be done for a given origin of electronic coordinates, and the resulting transition probabilities, as well as the atomic energies $E_f^{(A,B)}(R;b,v)$, depend on this origin. However, for our purposes the important point is that, for any origin, we may use the previous reasonings to explain why molecular expansions are able to describe ionization.

On the other hand, it is worth mentioning that the situation is radically different for a plane-wave-modified atomic expansion [18,19], which, when improved with the inclusion of pseudostates [20], can be written as a truncated version of Eq. (16) [the logarithmic phases in (3) and (4) usually being absorbed in the expansion coefficients]

$$\Psi_i^+(\mathbf{r},t)\approx\sum_{n=1}^{N_A}c_n^A(t)\Phi_n^A(\mathbf{r},t)+\sum_{n=1}^{N_B}c_n^B(t)\Phi_n^B(\mathbf{r},t)+\sum_{\alpha=1}^{N_{\rm ion}}c_\alpha^{\rm ion}(t)\Phi_\alpha^{\rm ion}(\mathbf{r},t). \tag{27}$$

Then, from our reasonings we see that wherever the expression (16) holds for the exact wave function, and since all bound-state traveling atomic orbitals $\Phi_n^{A,B}$ have either $E_n^{(A)}=E_n^A<0$ or $E_n^{(B)}=E_n^B<0$ [Eq. (14)], they represent either excitation or charge exchange, respectively, while pseudostates $\Phi_\alpha^{\rm ion}$ of positive energies (15) describe ionization. In particular, in the region where overlap effects are negligible there is no contamination of charge-exchange transition probabilities by ionization. The main consequence is that the correct fall of the corresponding cross sections at high energies is achieved when no pseudostates are introduced in the basis. A related case is furnished by plane-wave-modified molecular expansions [18,21,22], whose success at higher v [1] has been attributed [23] to their acting as an intermediate representation between plane-wave-modified atomic expansions and CTF-modified molecular ones. However, as stressed in [23] and [2], there is no guarantee that the success applies to other reactions or larger bases since the method is not rigorously *ab initio*.

III. ANALYSIS OF THE IONIZATION AND TRAPPING MECHANISMS

A. Computational method

In the present work we solved Eq. (1) by employing expansions (17) in terms of exact eigenfunctions of the electronic Hamiltonian, often called one-electron diatomic molecule (OEDM) orbitals:

$$H\chi_{nlm}(\mathbf{r},R)=E_{nlm}(R)\chi_{nlm}(\mathbf{r},R), \tag{28}$$

which are labeled according to the spherical-state quantum numbers (nlm) of their united-atom limit; for the degenerate states corresponding to a given $|m|\neq 0$, only the combination that is symmetric with respect to reflection through a plane containing the internuclear axis was employed, and will be labeled with $m>0$. Whenever useful, we shall also label these states according to the separated atom $\mathrm{Li}^{2+}(\eta)$ or $\mathrm{H}(\eta)$ limit. The CTF $U(\mathbf{r},t)$ in (17) is chosen to be the same as in previous work [24,25,2]:

$$U(\mathbf{r},t)=f(\mathbf{r},R)\mathbf{v}\cdot\mathbf{r}-\tfrac{1}{2}f^2(\mathbf{r},R)v^2t,\qquad f(\mathbf{r},R)\equiv f_\alpha(\mathbf{r},R)=\tfrac{1}{2}[g_\alpha(\mu)+d], \tag{29}$$

where

$$g_\alpha(\mu)=\alpha^{\alpha/2}\frac{\mu}{(\alpha-1+\mu^2)^{\alpha/2}} \tag{30}$$

and $d=1-2p$ (where p defines the position of the origin of electronic coordinates; see the beginning of Sec. II), $\alpha=1.25$ is a parameter chosen as in [2], and $\mu=(r_A-r_B)/R$ is the prolate spheroidal coordinate. The CTF (29) fulfills (18) and (19) and yields transition amplitudes that are origin independent. The numerical techniques employed to calculate the modified nonadiabatic couplings and integrate the system of differential equations for the expansion coefficients $a_{nlm}(t)$ are the same as in [2].

The energies of the traveling orbitals $\exp[iU(\mathbf{r},t)]\chi_{nlm}$ with respect to the moving atoms, $E_{nlm}^{(A,B)}(R;v,b)$, as defined in (24) and (25), were calculated by evaluation of the expressions

$$E_{nlm}^{(A,B)}=\left\langle\chi_{nlm}\left|-\frac{1}{2}\nabla^2-\frac{Z_{A,B}}{r_{A,B}}\right|\chi_{nlm}\right\rangle+\tfrac{1}{2}\langle\chi_{nlm}|(\nabla U_{A,B})^2|\chi_{nlm}\rangle, \tag{31}$$

which was carried out by factorization into one-dimensional integrals for the (λ,μ,ϕ) prolate spheroidal coordinates, followed by a 20-point Gauss-Laguerre quadrature for the λ integral and 48-point Gauss-Legendre quadrature for the μ integral. From (21) and (22) it is easy to see that these energies are independent of the parameter d defining the CTF in (29) since

$$U_A=(f+p)\mathbf{v}\cdot\mathbf{r}-\tfrac{1}{2}(f^2-p^2)v^2t \tag{32}$$

$$=\tfrac{1}{2}(g_\alpha+1)\mathbf{v}\cdot\mathbf{r}-\tfrac{1}{8}(g_\alpha+1)^2v^2t \tag{33}$$

and

$$U_B=(f-q)\mathbf{v}\cdot\mathbf{r}-\tfrac{1}{2}(f^2-q^2)v^2t \tag{34}$$

$$=\tfrac{1}{2}(g_\alpha-1)\mathbf{v}\cdot\mathbf{r}-\tfrac{1}{8}(g_\alpha-1)^2v^2t. \tag{35}$$

On the other hand, when the switching function f of (29) is multiplied by a strong cutoff function, as explained in Sec. II to deal with the case of a molecular expansion without translation factors, Eq. (31) is still valid, as well as (32) and (34). However, (33) and (35) no longer hold and the energies $E_{nlm}^{(A,B)}$ depend upon the value of the parameter d chosen in (29). Also, it is simpler to calculate these energies by directly using the expressions (24) and (25) with $U\equiv 0$:

$$E_{nlm}^{(A,B)}=\langle\chi_n|h'_{A,B}|\chi_n\rangle=\left\langle D_{A,B}\chi_{nlm}\left|-\tfrac{1}{2}\nabla^2-\frac{Z_{A,B}}{r_{A,B}}\right|D_{A,B}\chi_{nlm}\right\rangle, \tag{36}$$

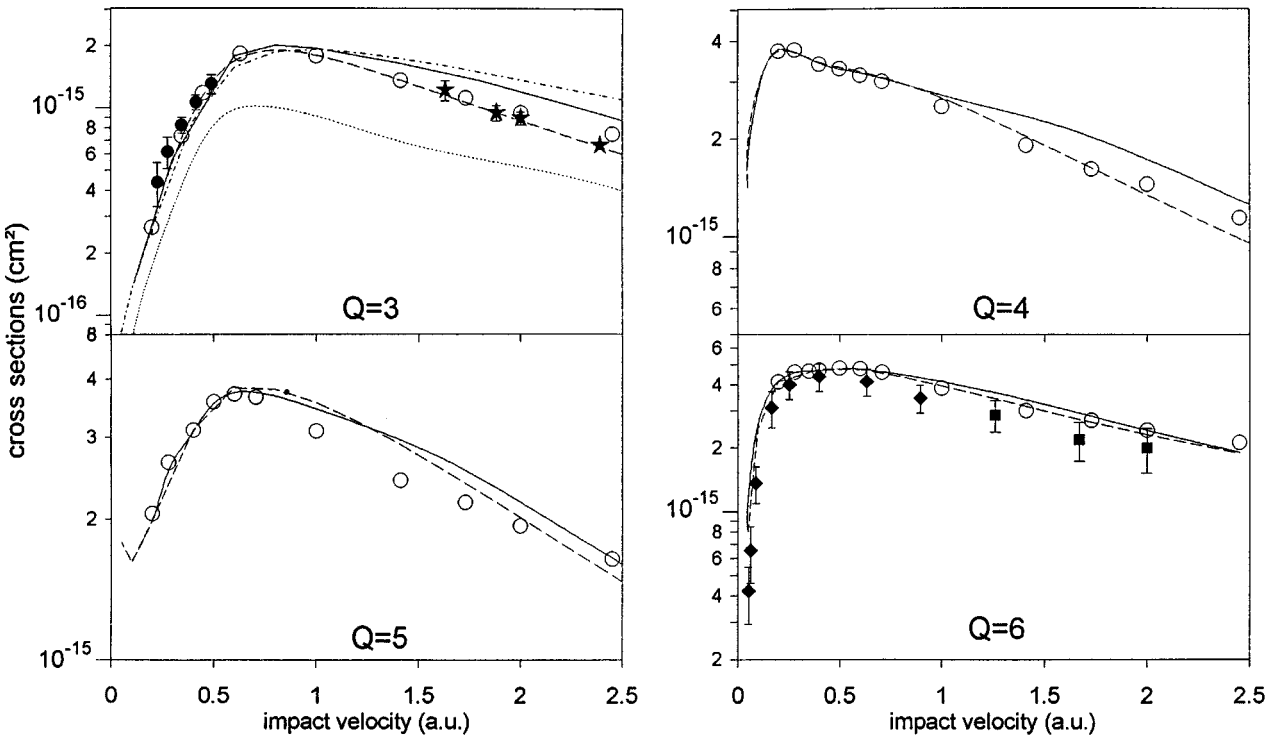

FIG. 1. Total capture cross sections for bare ion $I^{Q+}+\mathrm{H}(1s)$ collisions ($Q=3,4,5,6$) obtained with minimal 11-, 21-, 36-, and 26-OEDM-orbital (dashed curves) and extended 90-, 96-, 96-, and 83-OEDM-orbital (continuous curves) basis sets, respectively. The dot-dashed and dotted lines ($Q=3$) correspond to a 90-state calculation without a translation factor and to the contribution of the $n(n-1)0$ and $n(n-1)1$ states to the total capture cross section within the CTF-corrected 90-state calculation. ○, PWTF-AO electron-loss cross sections of Toshima [26]. Experimental data: ●, total capture of Seim *et al.* [28]; ⋆, electron-loss of Shah, Goffe, and Gilbody [27,29]; ◆ and ■, total capture and electron loss of Phaneuf, Janev, and Pindzola [30].

where the d dependence appears from (7) and (8) with $d=1-2p$.

B. Generality of previous findings: Electron-loss cross sections

We have performed calculations for $I^{Z+}+\mathrm{H}(1s)$ collisions, involving bare ions I^{Z+}, with $Z=3$–6 in the velocity range 0.05 a.u.$<v<$2.5 a.u. and expansions in terms of basis sets of increasing size. We display in Figs. 1(a)–1(d) for $Z=3$–6, respectively, our results for total capture cross sections obtained with ''minimal'' [3] (consisting of 11, 21, 36, and 26 OEDM orbitals, respectively) and ''extended'' (with 90, 96, 96, and 93 OEDM orbitals) basis sets. As in the case $Z=2$, presented in [2], our results show good agreement with available theoretical [26] and experimental [27–30] data for electron loss. The agreement holds even for the minimal sets and also for expansions without translation factors, whose data are also included in Fig. 1(a) as an illustration. Hence, at high v molecular expansions can yield remarkably accurate ionization cross sections and must therefore describe ionization. Our aim in the following sections is to analyze the origin and characteristics of this description.

Because of the similar characteristics of the electron-loss cross sections calculated for the various systems, and for the sake of conciseness, we shall focus, in the following, on the case of $\mathrm{Li}^{3+}+\mathrm{H}(1s)$ collisions as a prototype for multicharged ion-atom collisions. For a clearer understanding of our explanations, the correlation diagram for the lowest energies $E_{nlm}(R)$ of the LiH^{3+} quasimolecule is displayed in Fig. 2. To ease identification, rather than drawing $E_{nlm}(R)$ directly, we have scaled these energies and display in the figure the corresponding effective quantum number $n_0(E_{nlm})=8^{1/2}|E_{nlm}|^{1/2}$ [31] as a function of the internuclear distance. The curves are labeled with both the (nlm) united-atom and $[\mathrm{Li}^{2+}(\eta)$ or $\mathrm{H}(\eta)]$ separated-atom notations. In addition, for a nuclear trajectory with velocity $v=2$ a.u. and impact parameter $b=0.1$ a.u., we indicate, for each (nlm) state, the domain of internuclear distances for which *both* atomic energies $E_{nlm}^{(\mathrm{Li,H})}>0$ [see Eq. (31)]: according to the discussion in Sec. II, and provided that the overlap between the relevant atomic functions $\Phi_{\eta}^{\mathrm{Li,H}}$ [see Eq. (16)] is sufficiently small, in that domain the corresponding traveling orbital $e^{iU}\chi_{nlm}$ is then able to represent an ionizing electron.

C. Temporal evolution of populations

An advantage of the molecular method is its capability of providing a description of the processes through an analysis of their ''history'' along selected trajectories, as given by the temporal evolution of the state populations. In the following, we have chosen a nuclear trajectory yielding a sizable value for the ionization probability P^{ion}, with $v=2$ a.u. and $b=2$ bohrs; this will hereafter be called *the* representative trajectory for conciseness.

For this trajectory, we illustrate the electron-loss mechanism by displaying in Figs. 3(a)–3(c) the population $P_{\eta}(Z)=\Sigma_{n,l,m}|a_{nlm}(t)|^2$ corresponding to the capture $\mathrm{Li}^{2+}(\eta)$ multiplets (see Fig. 2), with $Z=vt$, and for basis

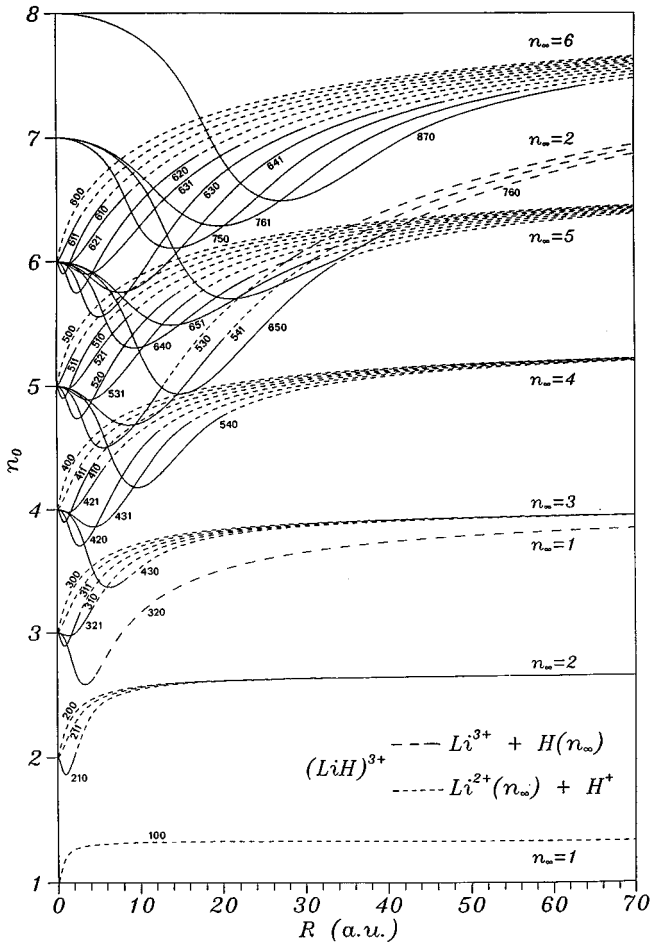

FIG. 2. Correlation diagram of the LiH^{3+} quasimolecule: effective quantum number $n_0(E_{nlm})=\sqrt{-8/E_{nlm}}$ as a function of the internuclear distance R. The continuous lines indicate, for the nuclear trajectory ($v=2$ a.u., $b=0.1$ a.u.), the domain of R for which both atomic energies $E_{nlm}^{(\mathrm{Li,H})}$ associated with the traveling molecular orbital $\chi_{nlm}e^{iU}$ are positive; see Eq. (31).

sets of 11 [Fig. 3(a)], 21 [Fig. 3(b)], and 33 [Fig. 3(c)] OEDM orbitals. The overall resemblance to the case of $He^{2+}+H$ collisions, described in [2], should be pointed out. Thus addition of the next ($\eta=4$) multiplet to the minimal (11-state) basis has the effect of absorbing part of the population of the lower ($\eta=3$) multiplet [Figs. 3(b) and 3(c)]; we see that this absorption takes place in two steps: at short R (in the region $Z\simeq 0$ bohrs) and at long R (for $Z\simeq 10$ bohrs). Then, in Fig. 3(c) this population is partly absorbed by the next ($\eta=5$) manifold, in both the short-R and long-R regions. We notice that in Fig. 3(b) the ($\eta=2$) capture population has practically converged with respect to further increase of the basis. Furthermore, we find that, for the three bases, the flux leaving the entrance channel and the electron-loss cross section remain sensibly the same.

Study of the temporal evolution of the state populations for larger basis sets shows the same pattern as in Figs. 3(a)–3(c): a short-R mechanism followed by a ladder-type [2] long-R process. In the following section we shall illustrate the latter process, which is simpler to analyze; it was partly described in [2], where, because of its sequential character, it was pictorially called a ''relay race'': the relay being the description of an ionizing cloud. Its relative contribution to the electron-loss cross section [shown in Fig. 1(a)] is ≈30% for $v=0.1$ a.u., rising to a maximum of about 46% for $v=1$ a.u. and decreasing further to ≈32% for $v=2.5$ a.u. As may be seen from Fig. 3, the first relay originates from the short-R mechanism, which is nonsequential and has not been explained before. In addition, this short-R mechanism produces a further 40–60 % of the electron-loss cross section, so that it is crucial in the description of the ionization process. Its analysis, which is considerably harder than that of the long-R process, is presented in Sec. III E.

D. Long-R (relay-race) mechanism

As explained in [2], this mechanism mainly takes place through transitions induced by radial couplings at pseudocrossings between the molecular energies $E_{n(n-1)0}$. According to Fig. 2, in these regions the atomic energies of Eq. (31) $E_{n(n-1)0}^{(\mathrm{Li,H})}>0$, so that the traveling orbitals $e^{iU}\chi_{n(n-1)0}$ are able to represent an electron that is unbound with respect to both nuclei. The process is illustrated in Fig. 4(a), where we have drawn the populations $P_{n(n-1)0}(Z)=|a_{n(n-1)0}(t)|^2$, along the representative trajectory and for an extensive 90-state calculation. In addition to this $n(n-1)0$ relay race, we have checked that rotational intramultiplet transitions stemming from the $n(n-1)0$ to the $n(n-1)1$ states appear, which are followed by a (less important) $n(n-1)1$ relay race.

The close connection between these mechanisms and the so-called T superseries transitions was already mentioned in [2]. In particular, the pseudocrossings involved are identical to the ''hidden crossings'' described in Ref. [9]. Nevertheless, as may have been expected, in actual calculations the process is more complex than the picture afforded by the T superseries. For example, relays are not entirely independent; an illustration is provided by the 650-760 and 650-870 relays in Fig. 4(a), which overlap because of the proximity of the corresponding pseudocrossings. More importantly, as stressed in [2], in an actual calculation the basis is finite: then, unlike the T superseries the relay-race mechanism cannot go on indefinitely and an (unphysical) accumulation of the corresponding flux in the top rung of the ladder appears; this is accompanied by a reflux of the population, affecting at least the penultimate rung, as may be seen from a comparison of Figs. 3(b) and 3(c) for the $\eta=3$ multiplet at $R\simeq 17$ a.u.

A more detailed description of the process is provided by the properties of the orbitals involved. As an illustration, we draw in Figs. 5(a)–5(h) the contours in the (x,z) plane for the χ_{430} [Figs. 5(a)–5(d)] and χ_{540} [Figs. 5(e)–5(h)] orbitals. While before the 430-540 pseudocrossing at $R\simeq 12$ bohrs (Fig. 2) the former has a sizable density in the internuclear region, after the pseudocrossing this property is exchanged with the χ_{540} density, while the χ_{430} orbital localizes around the projectile. Then, after the next 540-650 pseudocrossing at $R\simeq 20$ bohrs the χ_{540} orbital also takes on an atomic (Li) character. At sufficiently high nuclear velocities, the delocalized character of the traveling orbitals $e^{iU}\chi_{430}$ and $e^{iU}\chi_{540}$ for $R<12$ bohrs results in that their atomic energies (24) and (25) $E_{430}^{(\mathrm{Li,H})}, E_{540}^{(\mathrm{Li,H})}>0$ (see Fig. 2) and they can represent an ionizing electron, while for 12 bohrs$<R<$20 bohrs, only the latter orbital has this property. We may then conclude from

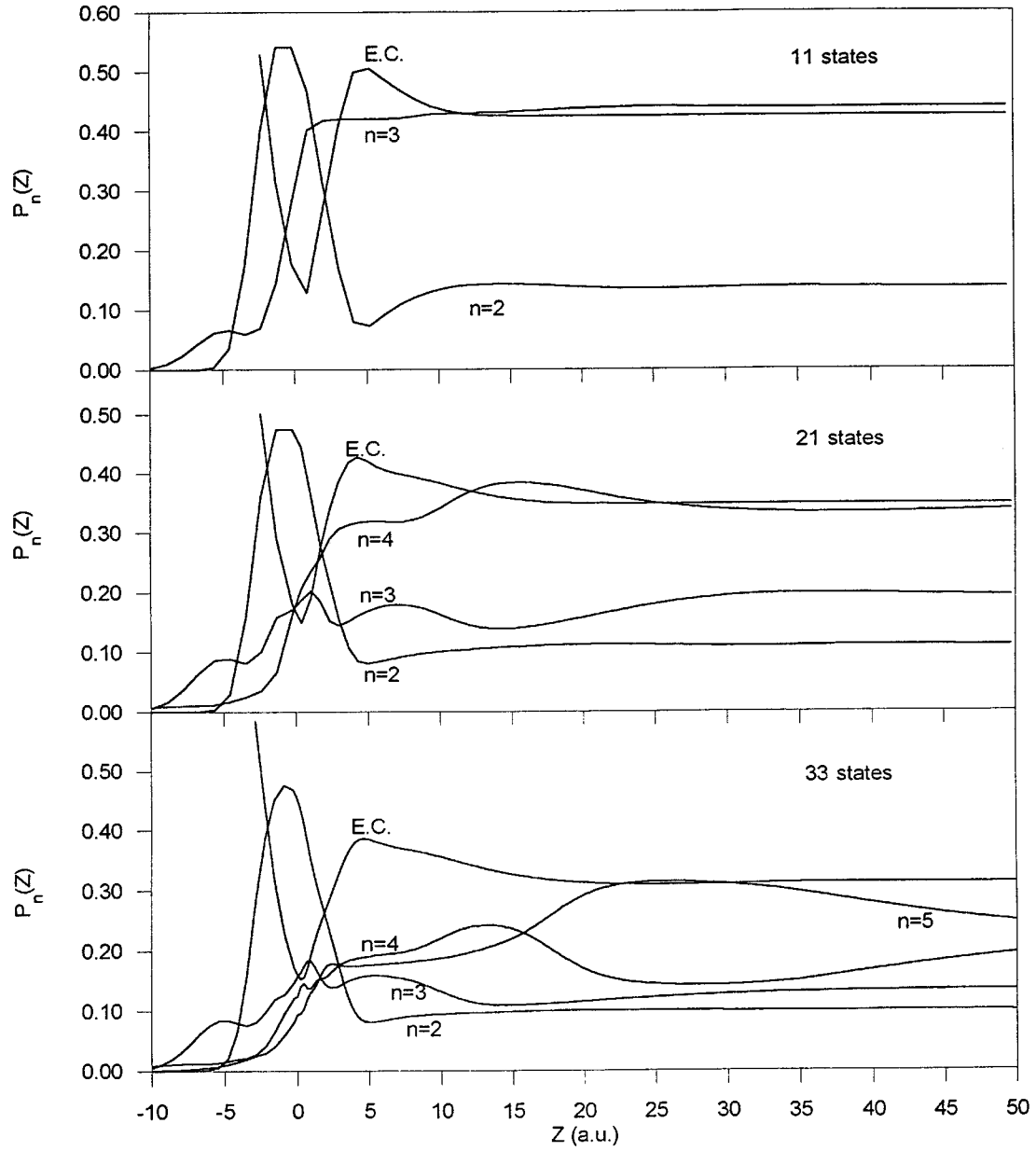

FIG. 3. Temporal evolution along the nuclear trajectory ($v=2$ a.u., $b=2$ a.u.) of the populations $P_\eta(Z)=\Sigma_{n,l,m}|a_{nlm}(Z)|^2$ for the capture $Li^{2+}(\eta)$ multiplets with $Z=vt$ and for basis sets of (a) 11, (b) 21, and (c) 33 OEDM orbitals. EC refers to the entry channel.

Figs. 2 and 4(a) that the relay race describes the evolution of a part of the ionizing wave function that is concentrated in the internuclear region. More specifically, in the long-R region, this wave function is mainly described: first, for $R<12$ bohrs, by the $e^{iU}\chi_{430}$ orbital; then, at the 430-540 relay, by $e^{iU}\chi_{540}$; and, as the nuclei recede farther from each other, by increasingly diffuse $e^{iU}\chi_{n(n-1)0}$ orbitals with positive atomic energies. Finally, the method fails when the last rung of the basis is reached, the ionizing wave function cannot be represented any longer, and the corresponding ionizing flux is trapped in a state with $E^{(\mathrm{Li,H})}_{n(n-1)0}<0$. The whole process can be visualized by comparison of Figs. 4(a) and 6, where in the latter we display the values of $E^{(\mathrm{Li,H})}_{n(n-1)0}(Z)$ along the representative trajectory. To avoid jumps in the 650 and 760 atomic energies of Fig. 6 and thus obtain neater graphs, the 650-760 pseudocrossing of Fig. 2 has been made diabatic.

Finally, we stress the fact that the previous mechanism can give rise to capture or ionization depending on the nuclear velocity. This is illustrated in Fig. 7, which displays the energy $E^{(\mathrm{Li})}_{540}(Z)$ for several nuclear velocities and shows that this state is only capable of describing the ionizing flux for $v\geqslant 1$ a.u.

E. Short-R mechanism

As mentioned in Sec. III C, this mechanism produces a sizable part of the electron-loss cross section and originates the relay race of Sec. III C. Because of its nonsequential character, to elucidate the characteristics of the processes involved requires a large number of calculations, in which specific couplings and sets of couplings are eliminated. Because of space limitations, it is unsuitable to present here all

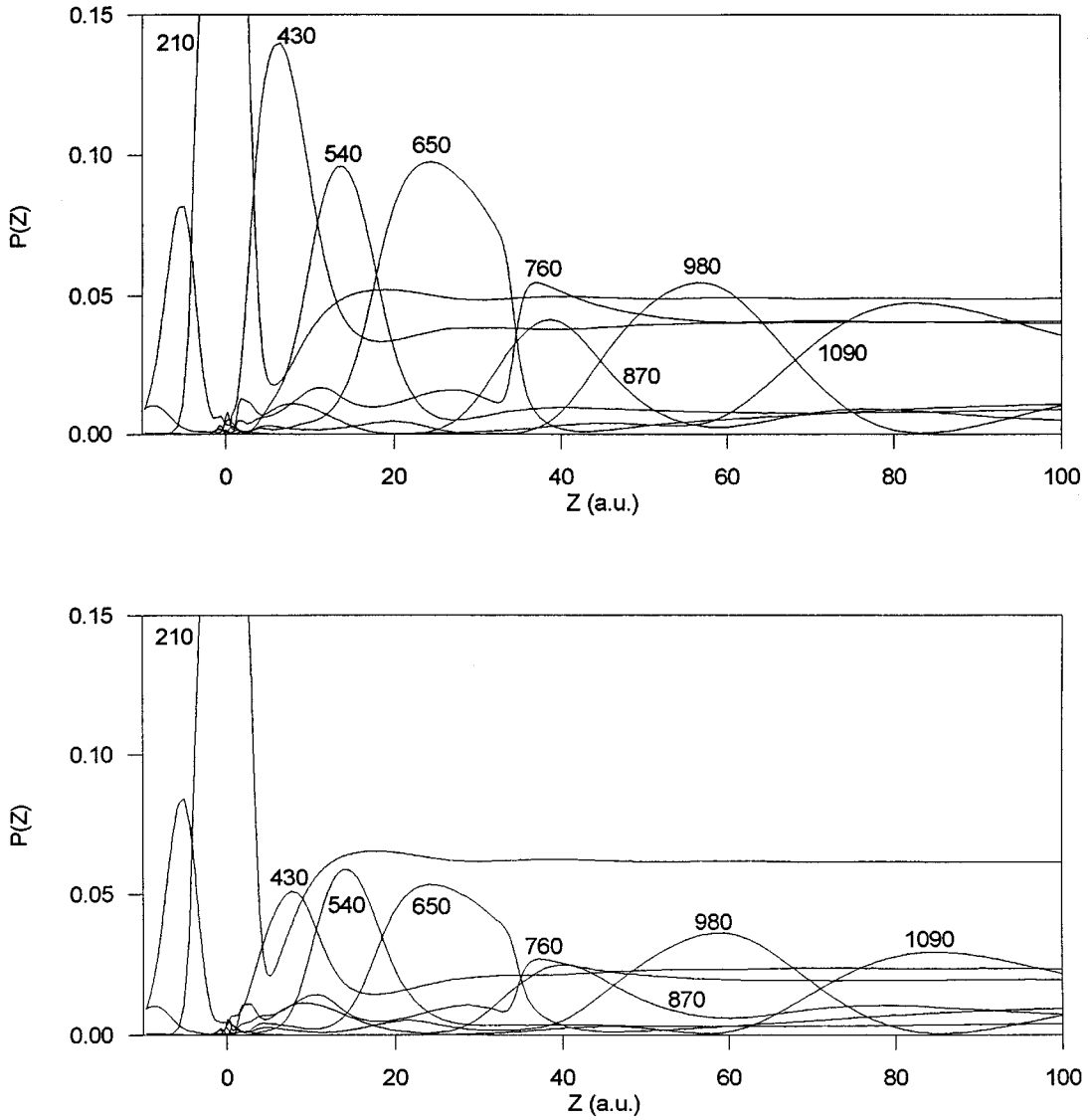

FIG. 4. Temporal evolution along the nuclear trajectory ($v=2$ a.u., $b=2$ a.u.) of the populations $P_{n(n-1)0}(Z)=|a_{n(n-1)0}(Z)|^2$ obtained by 90-state calculations in which the 431-430 rotational coupling (b) is or (a) is not canceled.

these results, so that we only state our findings and display the most compelling illustrations.

In these illustrations, we shall first consider the simplest, minimal, 11-state calculation. For the representative trajectory, we have plotted in Fig. 8(a) the populations of the $Li^{2+}(\eta=3)$ multiplet states, with united-atom quantum numbers 300, 310, 321, and 430. We see that for $Z>0$ the main outcome is an exit through the 300 channel. This flux arises from 321-300 rotational transitions, with the 321 state in turn being populated from the 320 and 210 ones. The rotational character of the process may be seen from Fig. 8(b), which displays the same populations as Fig. 8(a) for calculations in which the 210-321 and 320-321 nonadiabatic interactions have been canceled: the exit through the 300 state is then drastically reduced.

Next, to investigate which part of the description provided by the short-R process is a physical one, we examine the ionizing character of the cloud. Figure 9(a) shows that the 321 and 430 states have positive atomic energies in the small-R domain (see also Fig. 2) and are therefore able to describe an ionizing cloud. On the other hand, we find that the atomic energy $E_{300}^{(\mathrm{Li})}<0$, so that the 300 state cannot represent an ionizing event. Consequently, the trapping of the ionizing flux by this state in Fig. 8(a) is unphysical.

For extended bases, the same behavior is obtained. Figure 9(b) shows that the ionizing property of the 321 and 430 states is shared by the 431, 420, 651, and 640 traveling orbitals (as before, the sharp 530-640 and 541-651 pseudocrossings have been made diabatic for the sake of clarity). Similarly, one finds a trapping of this cloud by the $n00$ states, with $n\geqslant 3$. We are therefore led to investigate the workings of the mechanism.

These workings hinge on a peculiar structure of the coupling matrix between the molecular wave functions in the short-R region. First, because of the fast localization of the $n(n-1)1$ orbitals as R increases, a coexistence appears, in the pertinent (short-) R domains where $E_{n(n-1)1}^{(\mathrm{Li,H})}>0$, of sizeable $n(n-1)1$-$n00$ and $n(n-1)1$-$n(n-1)0$ rotational couplings. Second, in addition to these π-σ interactions, the channels in the σ and π manifolds interact between themselves through radial couplings, in the same region. All these

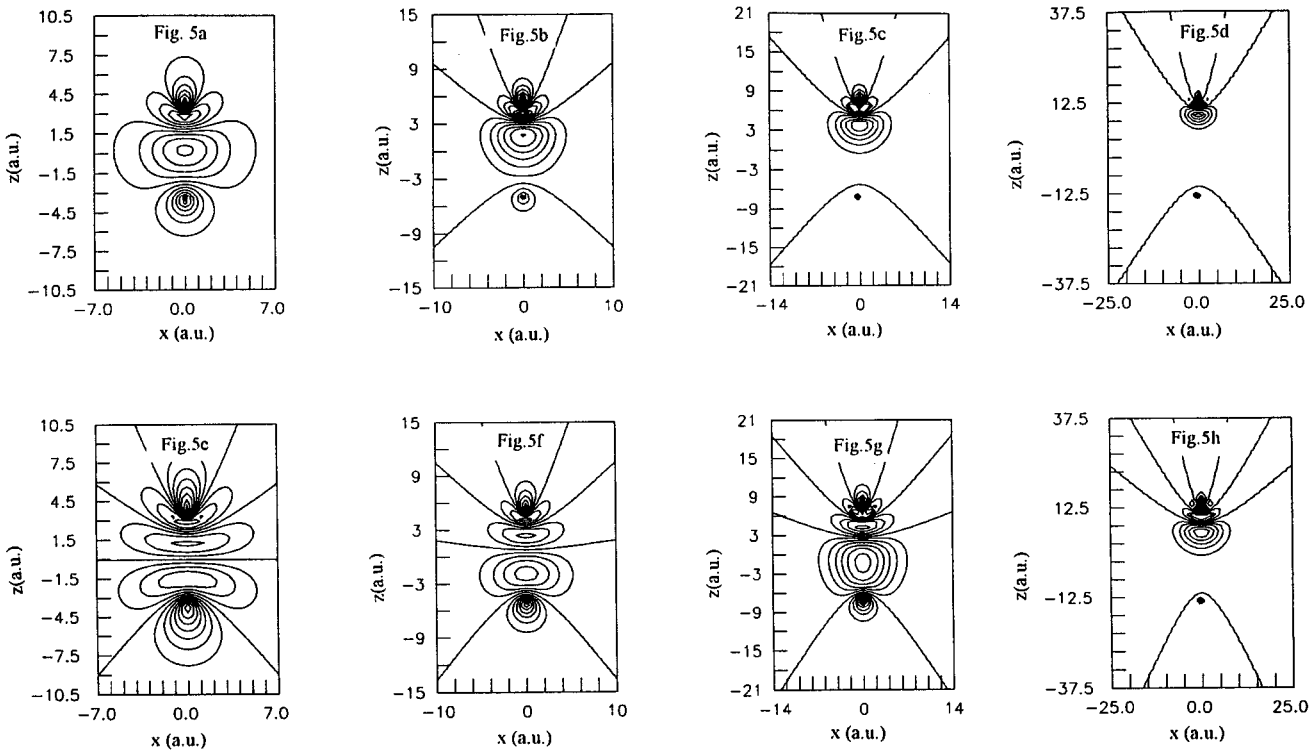

FIG. 5. Contours in the (x,z) collisional plane of (a)–(d) $\chi_{430}(x,y=0,z,R)$ and (e)–(h) $\chi_{540}(x,y=0,z,R)$ for several internuclear distances: (a) and (e) $R=7$ a.u., (b) and (f) $R=10$ a.u., (c) and (g) $R=14$ a.u., and (d) and (h) $R=25$ a.u. The black points indicate the nuclei positions.

couplings gives rise to a dense network of highly interconnected states in a small R domain, whose lowest tracks are schematically drawn in Fig. 10, which should be studied in combination with the quantitative energy diagram of Fig. 2.

It is significant that the network of Fig. 10 accounts for most of the ionizing flux: the rest corresponds to further intramultiplet distributions at large R. For example, for the 90-state calculation, the sum of the short-R $[\Sigma_n(\sigma_{n00}+\sigma_{n10}+\sigma_{n11})]$ and relay-race $[\Sigma_n(\sigma_{n(n-1)0}+\sigma_{n(n-1)1})]$ partial cross sections (in an obvious notation) accounts for about 90% of the electron-loss cross section for $v<1.8$ a.u., decreasing to about 80% at higher nuclear velocities.

We indicate in Fig. 10 that the network feeds from the 320 entrance channel (mixed with the 210 state at short R) would extend indefinitely up to and including the molecular continuum. Through the $\chi_{n(n-1)1}$ wave functions, it provides a representation of the π component of the expanding ionizing cloud. However, truncation of the basis results in that this representation is impaired and the part of the flow that does not feed the long-R mechanism accumulates in the dead ends of the network, which are the $n00$ states. A practical consequence of the simultaneous interconnection between the network elements is that cancellation of a given coupling results in that the probability flows through the others; this is the main feature that renders the analysis so difficult.

It may be seen in Fig. 10 that a very important feature of the short-R network is that in the way out of the collision it provides most of the input flux for the 430-540 relay-race mechanism, through the 320-431 and 431-430 rotational transitions. It can also be noticed in Fig. 10 that the 430 and 431 states belong to both short- and long-R mechanisms. Now, since, on the other hand, the former is a member of the 320-430-540-$\cdots$ T superseries and, on the other, it is transiently populated in Fig. 4(a) [and in Figs. 8(a) and 8(b) for the minimal basis] for $Z<0$ in a region where $E_{430}^{(\mathrm{Li,H})}>0$, it may seem surprising that it is fed in the long-R mechanism through a rotational coupling (Fig. 10).

In order to understand the dual role of the 430 state, we first analyze the transitions populating it for $Z<0$. These operate through the 320-430 coupling, which displays a maximum at $R\approx 8$ a.u. and changes sign at $R\approx 5.5$ a.u.; this change of sign explains the depopulation of the state near $Z=0$. Second, to show that the long-R mechanism is not triggered by this coupling but by the 431-430 interaction, we display in Fig. 4(b) the same collision history as Fig. 4(a), but with this interaction eliminated: a drastic reduction of the 430-540-$\cdots$ relay flux for $Z>0$ is then obtained, while the maximum of the 430 population for $Z<0$ is unchanged.

We now present a general proof that the short-R mechanism is essentially a rotational one and describes ionization. We display in Fig. 11, for the prototype trajectory and the 90-state calculation, the result of eliminating from the basis all orbitals of π symmetry with positive atomic energies, while keeping the negative-energy (χ_{n11}) π orbitals. An important lowering of the $\Sigma_n P_{n00}$ probabilities ensues, which shows that the former traveling orbitals, which can represent ionization, are indeed crucial in the process. Incidentally, we also see from Fig. 11 that an overcompensation for the elimination of ionizing π states appears, so that the mechanism involving σ states (and, as a consequence, the relay race)

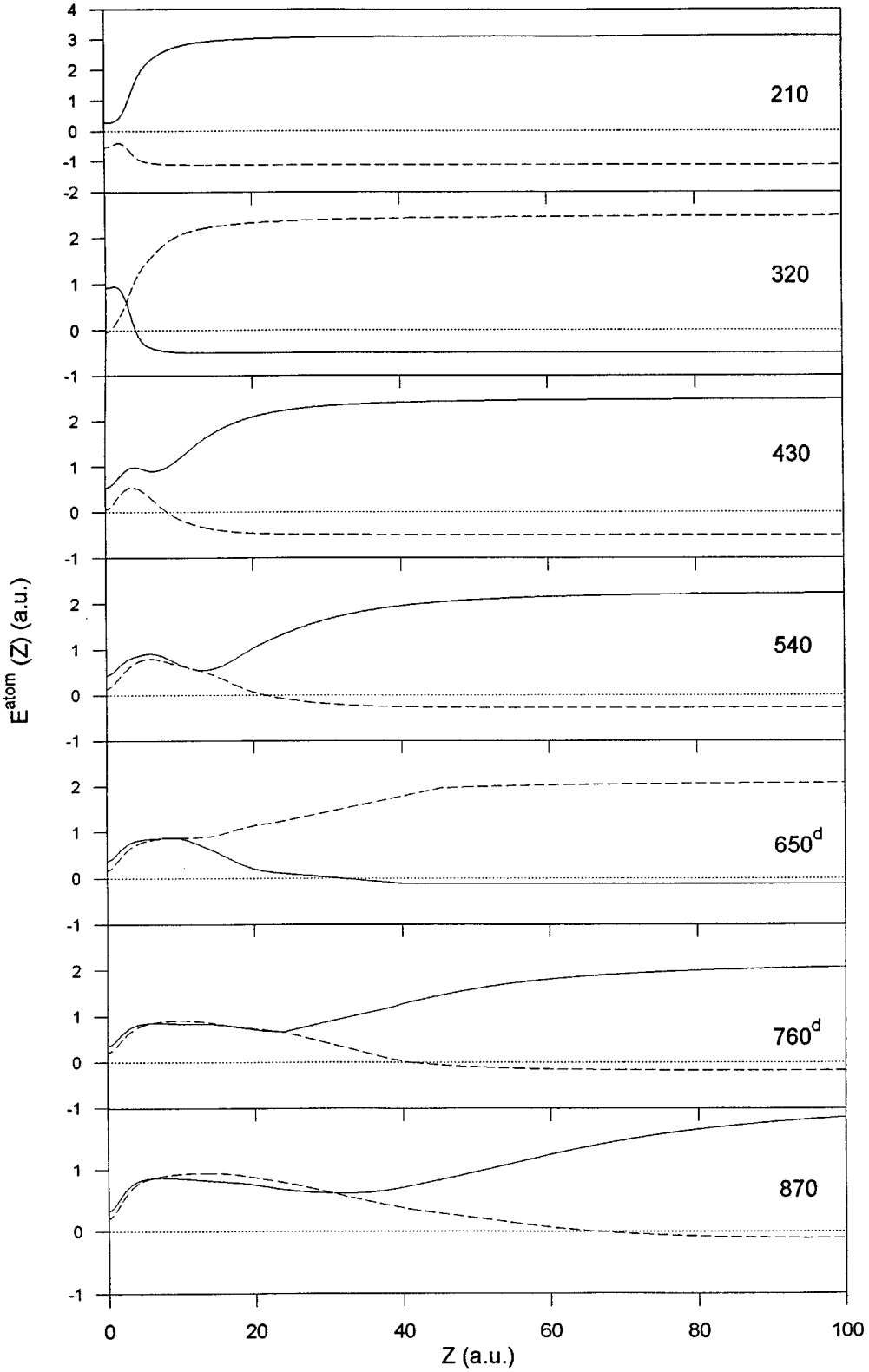

FIG. 6. Atomic energies of $\chi_{nlm}e^{iU}$ traveling molecular states in moving H (continuous lines) and Li (dashed lines) atomic frames as functions of $Z=vt$ for the nuclear trajectory ($v=2$ a.u., $b=2$ a.u.).

becomes much more efficient ($\Sigma_n P_{n(n-1)0}$ substantially increases).

Finally, from all the information gathered on the short-R mechanism and from the characteristics of the wave functions, we can conclude on the physical origin of the process and its relation with the relay long-R one. Both mechanisms share a common physical origin: the swift nuclei leave behind the electronic cloud as they separate and when this cloud has a positive energy with respect to both atoms, it describes an ionizing event. The difference is that the short-R mechanism arises from the inertia of the cloud to follow the rotation of the internuclear axis, while the relay race refers to nuclear translation. The superposition of traveling π and σ orbitals stemming from both processes then represents an ionizing cloud that is situated in the internuclear region, with its center off the internuclear axis.

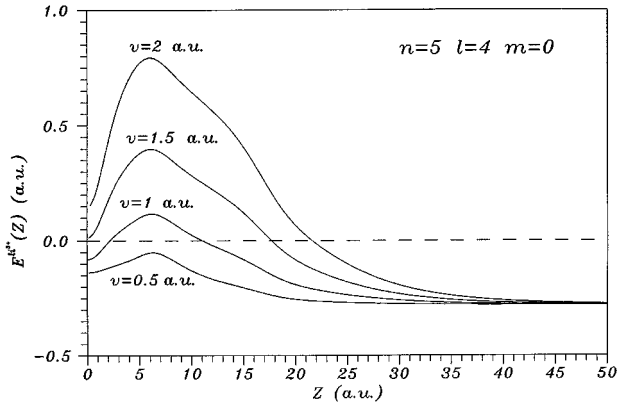

FIG. 7. Atomic energy of the $\chi_{540}e^{iU}$ traveling molecular state in the moving Li atomic frame as a function of $Z=vt$ for various nuclear velocities and $b=2$ a.u.

F. Molecular approach without translation factors

As mentioned in Sec. II the behavior of such an expansion is less definite than the CTF-modified one (17) because the results depend on the origin of electronic coordinates chosen in Eq. (1). Nevertheless, it is interesting to illustrate some similarities and differences with the previous case; we now do so for two choices of origin.

When the same OEDM orbitals $\{\chi_{nlm}\}$ are involved in the expansions with and without the CTF $\exp(iU)$, in the present context the pertinent differences lie with the atomic energies (31) and (36). We are thus led to consider the equivalent to, e.g., Fig. 6 for $E_{nlm}^{(\mathrm{Li,H})}(Z)$. For $p=\frac{1}{2}$ (origin at the geometrical center), these curves are shown in Fig. 12 for the $n(n-1)0$ states. Another possibility is to take $p=0$ (origin on the H nucleus), which permits one to correctly impose the initial condition because then $D_A=1$ in Eq. (7); the corresponding atomic energies are drawn in Fig. 13.

The first conspicuous difference between Figs. 6 and 12 is that, at large distances, in the former figure we have either $E_{n(n-1)0}^{(\mathrm{Li})}<0$ (capture channels) or $E_{n(n-1)0}^{(\mathrm{H})}<0$ (excitation channels), whereas in Fig. 12 (save for the 210 state) both $E_{n(n-1)0}^{(\mathrm{Li})}$ and $E_{n(n-1)0}^{(\mathrm{H})}\geqslant 0$ at large R. The reason is that the limit forms of the molecular wave functions $\chi_{nlm}(\mathbf{r},R)$ are superpositions of bound and continuum atomic wave functions $\Phi_f^{\mathrm{Li}}(\mathbf{r},R)$ or $\Phi_f^{\mathrm{H}}(\mathbf{r},R)$ [defined in Eq. (3)]. The same holds for Fig. 13, except for the excitation channels, for which $\chi_{nlm}\rightarrow\phi_\eta^{\mathrm{H}}$ as $R\rightarrow\infty$. Then, since $D_A=1$, we have from (36) that $E_{nlm}^{(\mathrm{H})}\rightarrow E_\eta^{\mathrm{H}}=-1/2\eta^2$. For instance, $\chi_{320}\rightarrow\phi_1^{\mathrm{H}}$, and $E_{320}^{(\mathrm{H})}<0$ for $R>4$ (see also Figs. 2 and 6).

From these reasons and the overall comparison of Figs. 6, 12, and 13, we see that the CTF greatly improves the physical sense of the basis orbitals, as is well known. Nevertheless, the most interesting feature for the present purposes is that in the small-R and hidden crossing regions, the atomic energies $E_{n(n-1)0}^{(\mathrm{Li,H})}(Z)$ of Figs. 12 and 13 exhibit a similar behavior to the case with translation factors (Fig. 6). Furthermore, we also have a similar network for the short-R rotational mechanism. Therefore, from all this we may expect an analogous, though less neat, description of ionization as

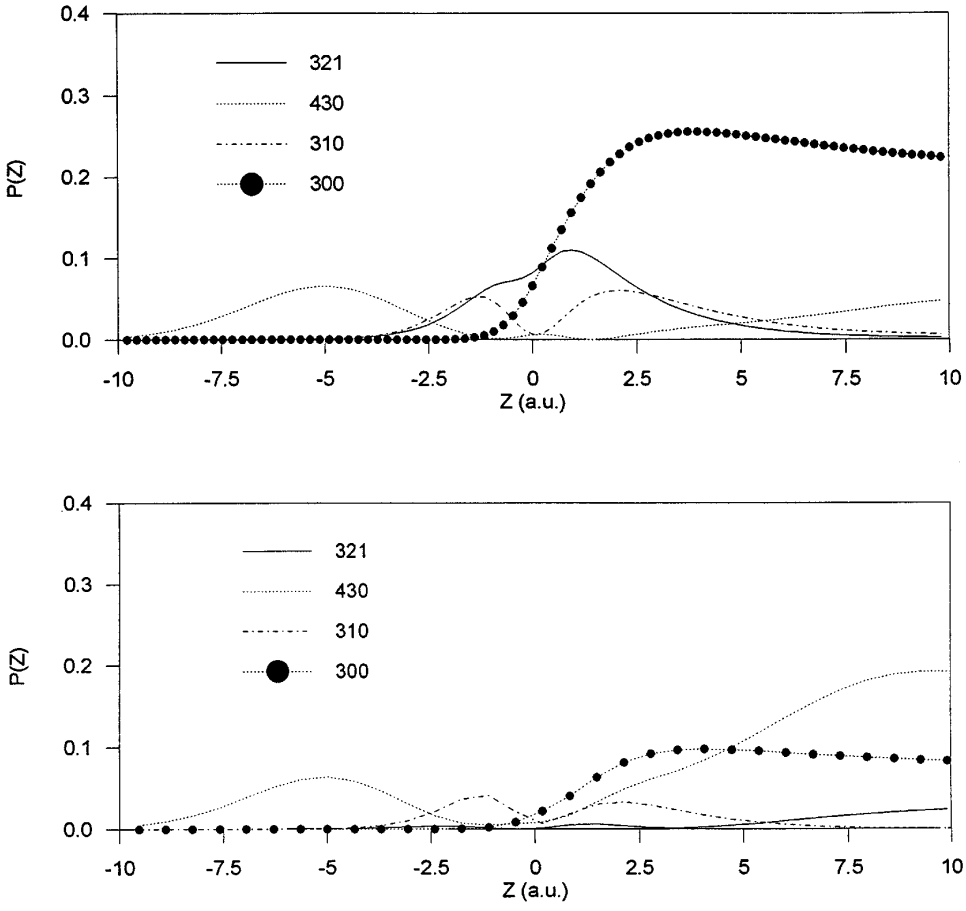

FIG. 8. Temporal evolution of the populations $P(Z)=|a_{nlm}(Z)|^2$ obtained (a) in the 11-state calculation and (b) in a modified 11-state calculation where the 210-321 and 320-321 rotational couplings are canceled.

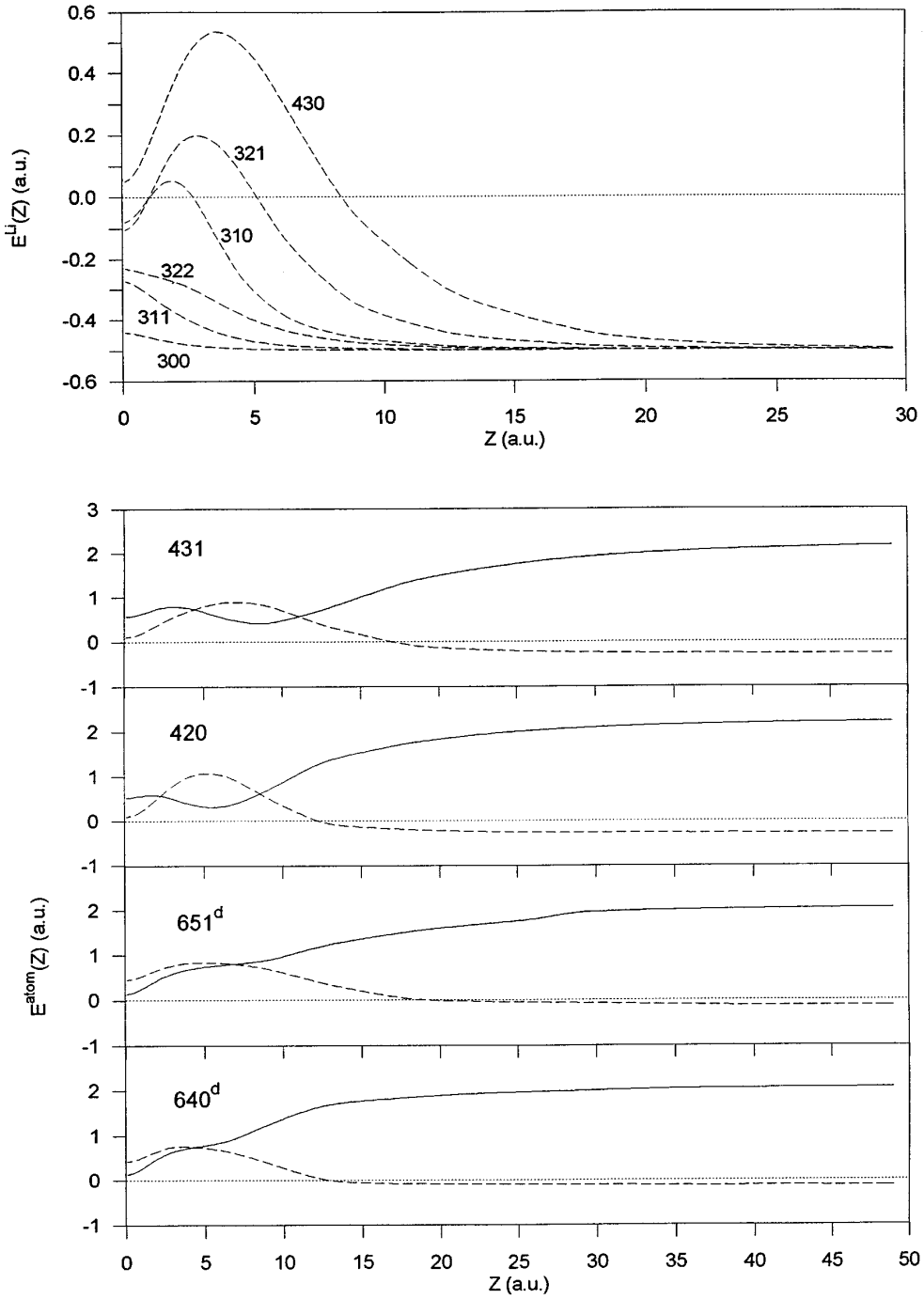

FIG. 9. Atomic energies of $\chi_{nlm}e^{iU}$ traveling molecular states in moving H (continuous lines) and Li (dashed lines) atomic frames as functions of $Z=vt$ for the nuclear trajectory ($v=2$ a.u., $b=2$ a.u.) (a) for all the states correlating asymptotically to $Li^{2+}(n=3)+H^{+}$ and (b) for higher excited states [431 and 420 correlating to $Li^{2+}(n=4)+H^{+}$ and 651^{d} and 640^{d} correlating to $Li^{2+}(n=5)+H^{+}$]. The sharp 541-651 and 530-640 pseudocrossings have been made diabatic for the sake of clarity.

when translation factors are employed. This was indeed shown in [2] for $He^{2+}+H$ collisions and may be seen in Fig. 1(a) for the present benchmark.

IV. CONCLUSIONS

To obtain information that will, in the future permit one to generate pseudostates in a systematic and physically meaningful way, we have attempted a detailed analysis of the description of atomic collisions by molecular close-coupling methods. We have first ascertained that our previous findings [2] on the $He^{2+}+H$ reaction hold generally for collisions between multicharged ions and $H(1s)$: while capture probabilities have the wrong fall at high velocity, the electron-loss (capture plus ionization) cross section is accurately given. We may thus answer in the positive question (iv) of the Introduction: the contamination of capture by ionization and the accurate description of the combined capture plus ionization process are general features of molecular close-coupling treatments in the intermediate-energy range.

To answer the other questions, we have presented a selection of a large number of tests carried out for the $Li^{3+}+H(1s)$ reaction. This system was chosen as a different benchmark from the usual $He^{2+}+H$ and as a prototype of multicharged ion-atom collisions.

With respect to question (i), in Sec. II B we have explained the apparent paradox of the description of ionization by expansions that do not include the three-body continuum: some wave functions represent both a bound molecular eigenstate in a fixed-nuclei frame of reference and atomic

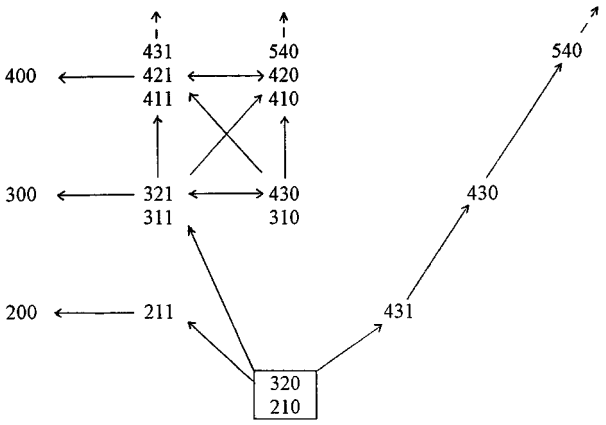

FIG. 10. Schematic of the lowest tracks of the network of molecular states implied in the transport and trapping of the ionizing flux.

unbound packet states in moving-nuclei frames. As explained at Sec. II C, this property is not shared by atomic basis functions modified with plane-wave-type translation factors and is, in general, not shared either by similarly modified molecular bases. Next, by using the atomic energies (24) and (25) in the moving frames as a tool, we have proved [Figs. 6, 7, 9(a), and 9(b)] the ionizing character of the traveling molecular states in the very regions where they are involved in nonadiabatic transitions. This explicit proof deals with point (ii) of the Introduction and is much more definite that a coincidence of calculated cross sections with ionization measurements in a specific case. By comparison of those figures with Fig. 8, the details of the ionizing mechanism can be understood from the velocity-dependent correlation diagram of Fig. 2.

Furthermore, our analysis, summarized in Secs. III D and III E, has not been restricted to a detailed confirmation of the conjectures of Refs. [1,2]: we also found that our previous (ladder) mechanism was significantly incomplete. A dominant part of the ionizing flux is due to a mechanism operating at short distances, which, in addition, is found to trigger (Fig. 10) the ladder one. Unlike the long-R process, the mechanism primarily involves *rotational* transitions and a closely knit network of strongly coupled states. This has important consequences regarding the requirements on pseudostates.

More specifically, in the long-R process the swift nuclei separate and leave behind a portion of the electron cloud in the internuclear region, in which the electron is unbound with respect to both nuclei. This portion is sequentially described by increasingly diffuse orbitals, which pass on the relay as soon as one of their atomic energies becomes negative. However, for a finite basis there is always a large enough distance such that the energies of all traveling orbitals become negative with respect to either one of the nuclei [Eq. (26)]. Then, as the nuclei separate the ionizing flux is trapped, almost exclusively in capture channels. Although some relay states are transiently populated in the way in of the collision [see, e.g., Fig. 8(a)], the relay ladder process is started by the short-R one, which arises from the reluctance of the electron cloud to follow the fast rotation of the internuclear axis. Because of the dense network of rotational and radial couplings that exist there, this gives rise to an almost simultaneous large number of transitions between the molecular states. In this case, incompleteness of the basis results in an unphysical trapping by the dead ends of the network, which also correlate to capture reaction channels. The final result is that the ionizing flux is accounted for as charge-exchange probabilities, and one obtains an overestimate of the capture cross sections at high velocity, while electron-loss cross sections are accurately reproduced.

We may thus answer point (iii) of the Introduction: the description of ionization by molecular states ceases to be a physical one when these states acquire a negative energy in a moving atomic frame and truncation of the basis prevents a description of the ionizing flux by the corresponding missing link in any of the chains of the network schematized in Fig. 10.

We may also partially answer question (iv): pseudostates

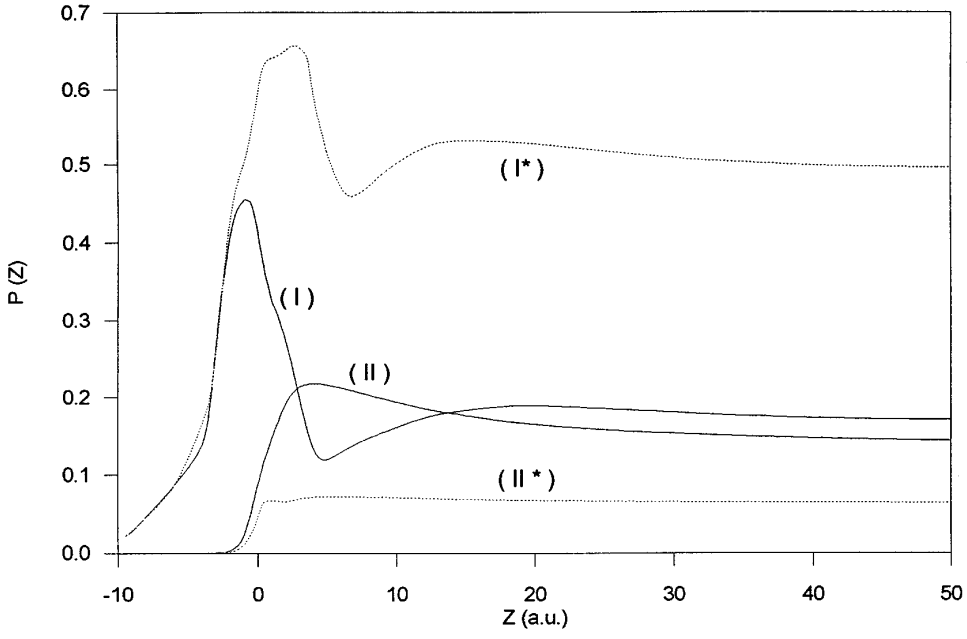

FIG. 11. Temporal evolution along the nuclear trajectory ($v=2$ a.u., $b=2$ a.u.) of the populations $\Sigma_n|a_{n(n-1)0}(Z)|^2$ and $\Sigma_n|a_{n00}(Z)|^2$ obtained in the 90-state calculation (I and II, respectively) and in a modified one with all orbitals of π symmetry with positive atomic energies eliminated from the basis (I* and II*, respectively).

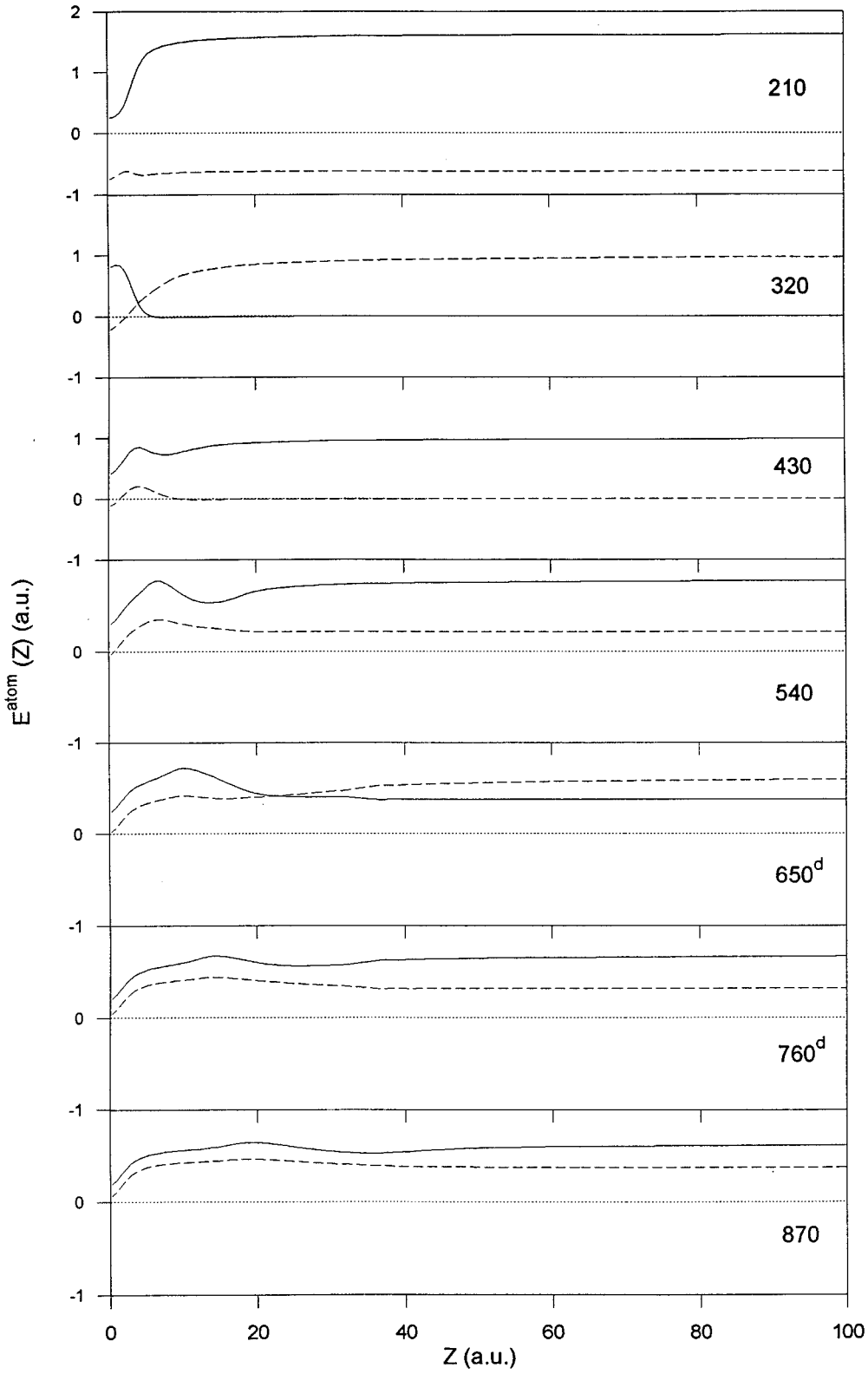

FIG. 12. Atomic energies of χ_{nlm} molecular states in moving H (continuous lines) and Li (dashed lines) atomic frames as functions of $Z=vt$ for the nuclear trajectory ($v=2$ a.u., $b=2$ a.u.). The origin of the calculation is at the geometrical center of the nuclei ($p=\frac{1}{2}$); see Eq. (36).

should complete the basis in such a way as to *locally* improve the description of both long- and short-R processes. This involves a wide range of internuclear distances in addition to the asymptotic region, and thereby a drastic change from the method of Ref. [4], which focused on this region (see Fig. 1 of [4]). The success of our method in the treatment of the $He^{+}+H^{+}$ reaction is probably due to the fact that the process is quasi-instantaneous and occurs at very short distances where completeness of the basis is best. Its partial failure in most other cases, including $He^{2+}+H$ and the present $Li^{3+}+H$ benchmark, is due to the fact that other internuclear distances are involved and consequently a different type of pseudostate is required, which should cover a region of configuration space lying between the nuclei and centered off the axis. In addition, the trapping by the $n00$ states found here was quite unexpected on physical grounds

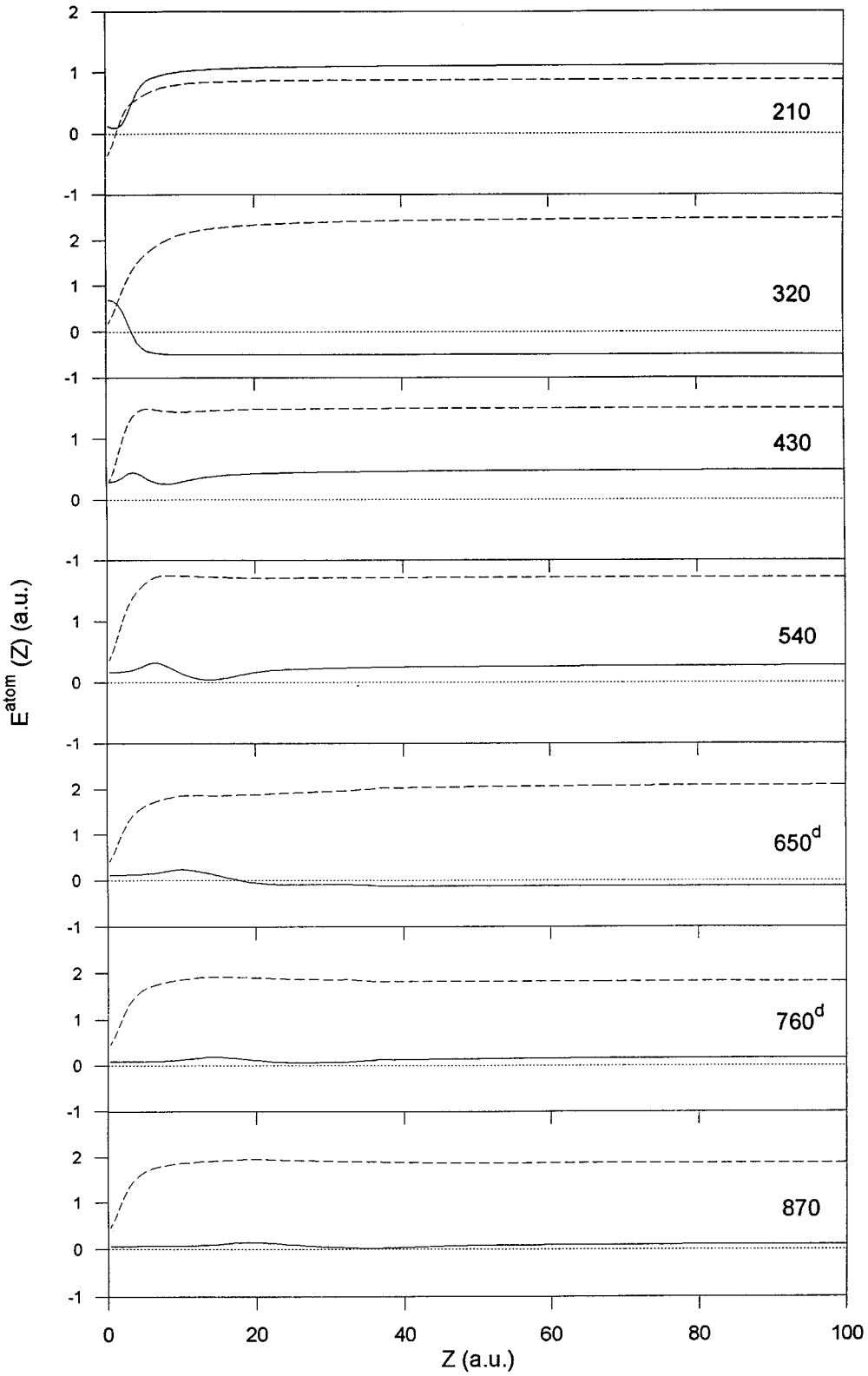

FIG. 13. Same as Fig. 12, but with the origin of the calculation at the H nucleus ($p=0$).

and should have a strong bearing on the optimal choice of pseudostates.

Finally, the present work offers a quantitative description of ionization at intermediate energies that is not available in the literature. In this respect, it should be noticed that, in spite of the complexities of the detailed mechanisms, the overall physical picture obtained is a very simple one. In this picture, ionization, like charge exchange or excitation, arises as a result of the inertia of the electron cloud to adiabatically follow the nuclear motion. This gives rise to nonadiabatic transitions, which can represent an ionizing flux whenever the nuclear velocity is high enough that the energy of the traveling orbitals is positive with respect to both moving atomic reference frames. Then, as the close-coupling treatment minimizes the difference between approximate and exact wave functions, it also represents the ionizing part of the

latter. This picture was obtained here for molecular expansions that incorporate, as usual, a common translation factor. Molecular expansions without translation factors share the same properties, although in a less neat way, showing that the factors greatly improve the physical character of the basis orbitals.

ACKNOWLEDGMENTS

This work has been partially supported by the DGICYT Project No. PB93-288-C02, the Centre National Universitaire Calcul (Montpellier, France), and the Sud de Acción Integrada Hispano-Francesa 396B.

[1] L. F. Errea, C. Harel, H. Jouin, J. M. Maidagan, L. Méndez, B. Pons, and A. Riera, Phys. Rev. A **46**, 5617 (1992).
[2] L. F. Errea, C. Harel, H. Jouin, L. Méndez, B. Pons, and A. Riera, J. Phys. B **27**, 3603 (1994).
[3] L. F. Errea, L. Méndez, and A. Riera, J. Phys. B **28**, 907 (1995).
[4] L. F. Errea, C. Harel, H. Jouin, L. Méndez, B. Pons, and A. Riera, Phys. Rev. A **52**, R2505 (1995).
[5] L. F. Errea, C. Harel, P. Jimeno, H. Jouin, L. Méndez, and A. Riera, Phys. Rev. A **54**, 967 (1996).
[6] S. B. Schneiderman and A. Russek, Phys. Rev. **181**, 311 (1969).
[7] J. Kuang and C. D. Lin, J. Phys. B **29**, 1207 (1996).
[8] J. M. Rost, J. S. Briggs, and P. T. Greenland, J. Phys. B **22**, L353 (1992).
[9] J. P. Grozdanov and E. A. Solov'ev, Phys. Rev. A **42**, 2703 (1990).
[10] M. Pieksma and S. Y. Ovchinnikov, J. Phys. B **24**, 2699 (1991).
[11] M. Pieksma and S. Y. Ovchinnikov, J. Phys. B **25**, L373 (1992).
[12] R. K. Janev, G. Ivanovsky, and E. A. Solov'ev, Phys. Rev. A **49**, R645 (1994).
[13] G. Bandarage and R. Parson, Phys. Rev. A **41**, 5878 (1990).
[14] B. H. Bransden and M. H. C. McDowell, *Charge Exchange and the Theory of Ion-Atom Collisions* (Oxford Science, Oxford, 1992).
[15] Dž. Belkić, R. Gayet, and A. Salin, Phys. Rep. **56**, 279 (1979).
[16] Dž. Belkić, J. Phys. B **10**, 3491 (1977).
[17] Yu. N. Demkov, *Variational Principles in the Theory of Collisions* (Pergamon, Oxford, 1963).
[18] D. R. Bates and R. McCarroll, Proc. R. Soc. London Ser. A **245**, 175 (1958).
[19] D. R. Bates, Proc. R. Soc. London Ser. A **245**, 299 (1958).
[20] P. G. Burke and T. G. Webb, J. Phys. B **3**, L131 (1970).
[21] G. J. Hatton, N. F. Lane, and T. G. Winter, J. Phys. B **12**, L571 (1979).
[22] T. G. Winter and G. J. Hatton, Phys. Rev. A **21**, 793 (1980).
[23] A. Riera, in *Time-Dependent Quantum Molecular Dynamics*, edited by J. Broekhove and L. Lathouwers (Plenum, New York, 1982), p. 311.
[24] C. Harel and H. Jouin, J. Phys. B **24**, 3219 (1990).
[25] C. Harel and H. Jouin, Europhys. Lett. **11**, 121 (1990).
[26] N. Toshima, Phys. Rev. A **50**, 3440 (1994).
[27] M. B. Shah, T. G. Goffe, and H. B. Gilbody, J. Phys. B **11**, L233 (1978).
[28] W. Seim, A. Mäller, I. Wirkner-Bott, and E. Salzborn, J. Phys. B **14**, 3475 (1981).
[29] M. B. Shah and H. B. Gilbody, J. Phys. B **15**, 413 (1982).
[30] R. A. Phaneuf, R. K. Janev, and M. S. Pindzola, *Atomic Data for Fusion* (Oak Ridge National Laboratory, Oak Ridge, TN, 1987), Vol. 5.
[31] K. Helfrich, Z. Phys. D **13**, 295 (1989).